Experimental Characterization of Thermal Conductance across the Separator-Shell Interface in Dry Cylindrical Lithium Ion Batteries

Aalok Gaitonde, Amulya Nimmagadda, and Amy Marconnet
School of Mechanical Engineering & The Birck Nanotechnology Center
Purdue University
West Lafayette, Indiana, U.S.A, 47907
Email: marconnet@purdue.edu

ABSTRACT

Although Lithium ion batteries offer numerous advantages (e.g. energy density, efficiency, etc.) over other types of batteries, recent accidents involving consumer electronics have necessitated a deeper understanding of the thermal behavior of these batteries. Thermal transport across the multilayer stacks that form prismatic and spiral-wound batteries generally hinders heat removal from the system. In cylindrical batteries, most commonly found in laptops, electric vehicles and power banks, heat must conduct to the metallic shell through many layers of the anode-separator-cathode structure, which is of low effective thermal conductivity. This work presents thermal conductance and thermal conductivity measurements of dry 18650 cells using infrared microscopy. Two-dimensional temperature maps are captured and are averaged in the direction normal to the heat flow for analysis of the one-dimensional temperature profiles. Interfacial temperature jumps indicate thermal resistances and can be separated from the thermal gradients due to conduction within a single material. We measure both cross-plane thermal conductivity of the battery stack and interfacial thermal conductance. Interfacial thermal conductance and the thermal conductivity in active batteries is expected to be higher, due to the presence of a liquid electrolyte. This work demonstrates that the low cross plane thermal conductivity of the plastic separator material is one of the limiting factors in heat dissipation.

NOMENCLATURE

A	area, m^2
d	diameter, m
h	heat transfer coefficient, $W/(m^2K)$
k	thermal conductivity, W/(mK)
L	length, m
q	heat flow rate, W/m
r	radius, m
R	thermal resistance, K/W

Subscripts

cond	conduction
conv	convection
i	inner
o	outer
th	thermal

INTRODUCTION

With the advent of hybrid vehicles and their increasing popularity, Lithium ion batteries have gathered prominence in the recent years. Though they were used in small scale devices from a long time, their applications in the automotive industry have caught the attention of many researchers. Even though Lithium ion batteries are sought after due to their high-energy densities when compared to other available batteries [1], their usage is limited by heat generation associated with continuous operation and the potential for thermally-driven failure. Past work has mainly focused on determining the electrochemical properties of these batteries. But the safety concerns related to the batteries have turned attention towards thermal aspects of these battery [2,3]. Work in both the experimental and computational domains has examined the internal heat generation rates and internal temperatures [4,5]. To better understand the thermal characteristics associated with the battery operation, researchers have often estimated various effective properties of the battery such as specific heat and thermal conductivity. Only a few recent studies have directly measured the thermal conductivity for batteries of different compositions [6,7] and for individual battery components such as the cathode and the anode [8,9]. Although the batteries are anisotropic, heat transfer across the numerous battery layers in the direction normal to the electrode stack is often the limiting factor in removing heat from the cell, due in part to the numerous interfaces and that heat removal occurs at the perimeter of the cell. Ultimately, improved data on thermal properties is needed to design batteries with improved performance and reliability.

Among the many thermal properties associated with a lithium ion battery, the effective cross-plane thermal conductivity of the battery electrode stack and the interfacial thermal conductance across the plastic separator (the outermost layer in the battery jelly roll) and the steel shell of the battery are of significant interest, since these parameters are key factors in determining internal temperatures, preventing thermal runway, and ensuring safety of the charging and discharging processes of the battery, especially at high current rates. Our recent measurements of the thermal conductance between the separator and the battery case, required complete dissection of commercial 18650 batteries to harvest the electrodes and measure the thermal properties *ex citu* [10]. In this work, we develop and validate a new method to measure the thermal conductance within an 18650-cylindrical battery cell in a geometry more faithful to operating conditions. Specifically, here we build a dry 18650 battery using the same electrodes that constitute a functional battery and measure the thermal properties using cylindrical version of the typical reference bar method integrated with an infrared microscope for high resolution temperature measurements.

EXPERIMENTAL METHODOLOGY

The diameter of a cylindrical 18650 Lithium Ion battery is 18mm, and the height is 18650 (and hence the `18-65-0' nomenclature). The individual electrodes are around 100 to 150 µm (depending on the chemistry and type), while the porous plastic separator is ~25 µm thick. At these length scales, it is challenging to spatially resolve temperature gradients across the stack in the radial direction with conventional thermal metrology tools (*e.g.* thermocouples, RTDs, etc.). Here, we use an infrared microscope with 1.8 µm spatial resolution to measure the temperature profiles within the battery stack during thermal property tests. In cylindrical batteries, heat transport is dominated by radial heat transfer, and the gradient along the vertical or axial direction is negligible, due to two factors: nearly uniform heat generation happening throughout the core of the battery [11] and the large aspect ratio (L/d ~ 3.6). Thus, we focus on characterizing the properties in the direction perpendicular to the electrode windings (*i.e.* the radial direction). The design and working of a cylindrical battery test rig is discussed in the following sections.

Design of a Cylindrical Battery Test Rig

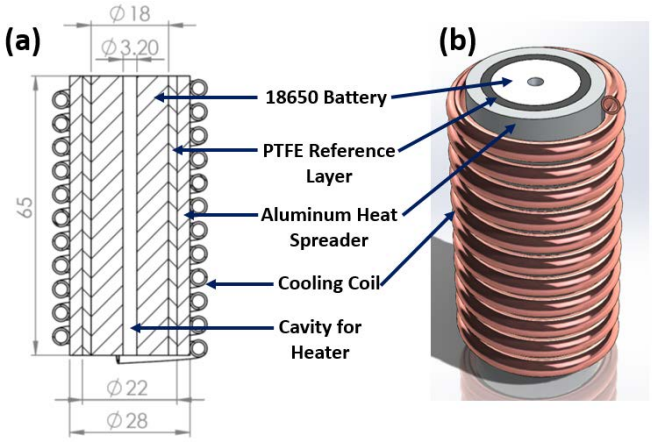

Fig. 1 (a) Cross-section view and (b) 3D model of the cylindrical battery test rig. The axial cavity in the center of the constructed battery holds a cartridge heater that establishes the temperature gradient across the electrode windings during thermal tests. The battery is enclosed inside a sleeve of PTFE (Teflon), which is used as a reference material to quantify heat flow through the battery. The PTFE sleeve is surrounded by an aluminum heat spreading sleeve, which is in contact with a cooling coil. All dimensions shown in (a) are in mm.

To measure the thermal conductivity of the battery and interfacial thermal conductance across the separator-case interface, a temperature gradient must be established in the radial direction. To achieve this, a dry battery is constructed with a cavity for insertion of a 60 Watt miniature cartridge heater (Firerod® Cartridge Heaters, Watlow GmbH) in the center of the cell (see Figure 1). To measure the heat rate in the system, the battery is enclosed in a cylindrical sleeve of a known 'reference' material. In this work, high temperature polytetrafluroethylene (PTFE), commonly and commercially known and available as Teflon [12], is used as the reference material. The thermal conductivity of this material k_{ref} is known, and is verified using a certified reference material for thermal conductivity from the National Institute of Standards and Testing [13]. The temperature distribution throughout the battery and in the reference material is recorded by an infrared microscope (Infrascope, Quantum Focus Instruments Corporation). By measuring the temperature gradient in the reference material, the heat flow rate through the system is given by

$$q_r = \frac{T_{ro} - T_{ri}}{\frac{\log\left(\frac{r_o}{r_i}\right)}{2\pi k_{ref}}} \qquad (1)$$

where T_{ro} and T_{ri} are the temperatures of the outer, r_o, and inner, r_i, edges of the reference layer, respectively.

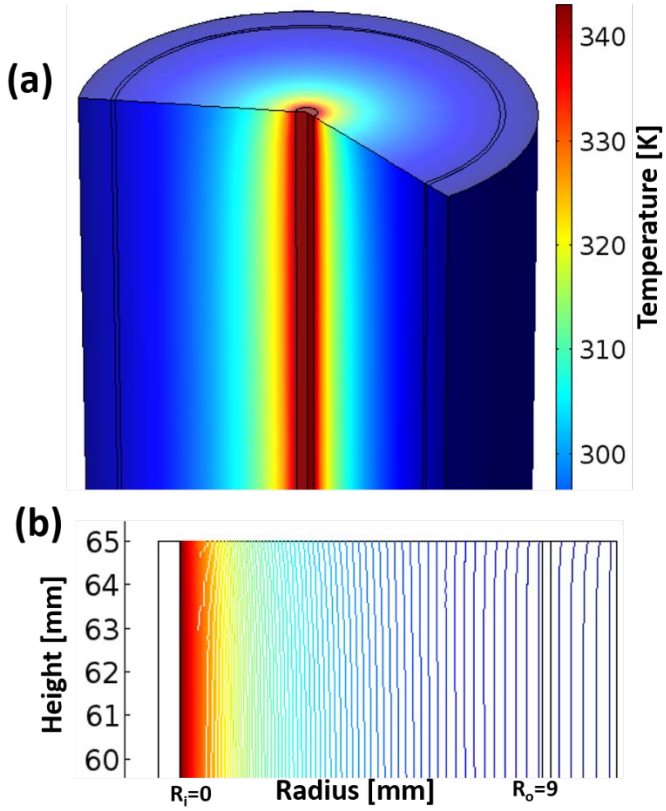

Fig. 2 (a) Predicted temperature distribution in a battery structure when heat is generated inside the central cavity, and (b) the corresponding isotherms near the top surface of the battery where the infrared images are recorded. The isotherms are reasonably parallel, which signifies that heat transport is approximately 1D in the radial direction, and that convection losses are insignificant.

While the cartridge heater generates heat in the core of the battery, the outer surface of the battery is cooled by the liquid flowing through the cooling coil, establishing a temperature difference across the battery stack. Specifically, the outer surface of the reference sleeve is enclosed by a cylindrical Aluminum heat spreading sleeve, which has a winding of copper tubes on its outer perimeter, and acts as a heat exchanger. The copper tubes are connected to heat spreading sleeve using thermal cement. A heat transfer fluid flows through the copper tubing to maintain the outer surface of the reference layer at the desired temperature. The battery, reference sleeve, and the aluminum heat spreading sleeve are concentric, with transition fits at their mating surfaces. Before assembly, the interfaces between these are smeared with a thermal interface material (TIM) to improve the thermal conductance across the interfaces.

Verification of design accuracy

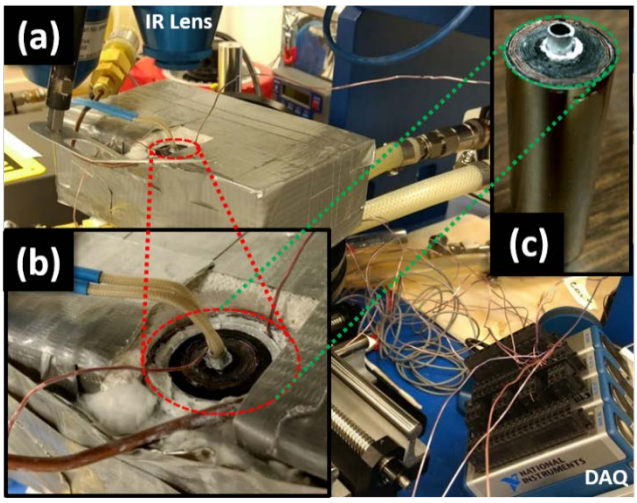

Fig. 3 (a) Overview of the manufactured test rig housed in a ceramic insulator brick. The IR microscope lens observes the top surface temperature throughout the test cell. (b) The test cell embedded in the ceramic brick with the cartridge heater leads running out from the top along with fine gauge thermocouples that monitor the extreme system temperatures *i.e.,* the hot side and the cold side temperature, for general reference only. The primary measurements are done by the infrared microscope, whose 1x objective lens is marked in the picture. (c) Constructed 18650 dry battery test cell that is housed in the cylindrical battery measurement rig in panel (b).

Before machining and manufacturing the test rig, the system was modeled as an axisymmetric system in a commercial finite element package, COMSOL Multiphysics®, to verify the performance and accuracy of the proposed design. The crucial parameters verified with the model are the heat flow paths, convection losses, and the effects of heat flow in the axial direction. To simulate the experiment, a constant temperature boundary condition is defined at the heater cavity, and a similar boundary condition is applied at the outer cold surface of the aluminum heat spreader. Since the experiments are conducted in air, the heat transfer coefficient from the top surface is varied as a parameter from 10 to 50 W/(m^{2}K), to check if convection losses from the exposed surfaces are significant. Figure 2(a) shows a sectional view of the results of the simulation, at steady state. Figure 2(b) shows the corresponding isotherms near the top surface of the battery, where the infrared measurements are recorded, and they are found to be reasonably parallel for the range of convection losses investigated. This is expected, since the thermal resistance to convection is approximately 20 times higher than the thermal resistance to conduction. Specifically, the thermal resistances are given by

$$R_{th,cond} = \frac{\log\left(\frac{r_o}{r_i}\right)_{battery}}{2\pi L k_{battery}} \; and \; R_{th,conv} = \frac{1}{hA} \qquad (2)$$

where $R_{th,cond}$ and $R_{th,conv}$ are the thermal resistances to conduction and convection, respectively, $k_{battery}$ is the predicted thermal conductivity of the battery stack, and h and A are the heat transfer coefficient and surface area exposed to convection, respectively. For a predicted effective thermal conductivity of the battery stack of 0.3 W/(mK), and a heat transfer coefficient of 15 W/(m^{2}K), the thermal resistances to conduction and convection are 13 K/W and 272 K/W respectively.

Manufacturing the test rig

Figure 3(a) shows the experimental setup with (b) the test rig embedded into a ceramic block for insulation and support. The battery jellyroll is constructed using electrodes, separator, and the 18650 metallic shells purchased from MTI Corporation, Richmond, CA. The battery cathode is a double side coated Aluminum foil with $LiFePO_4$, while the anode is a single side coated copper foil with CMS graphite. The aluminum and copper act as current collectors, whereas the coatings are the active materials. The plastic porous separator is 25µm thick, and is made out of polypropylene. Long strips are cut to size, and then rolled along until the diameter of the roll becomes 18mm, after which it is pushed into the empty 18650 shell, as shown in Figure 3(c). The reference sleeve is machined from a block of black PTFE, while the heat spreading sleeve is machined from aluminum. After the rig is assembled, it is placed in a ceramic block that serves two purposes: (1) it acts an an insulator, keeping the heat exchanger from losing heat to the ambient air, and (2) it keeps the rig aligned vertically under the microscope. Swagelok compression fittings connect the ends of the coil heat exchanger to the constant temperature fluid bath, and ensure a leak proof and removable connection. Two fine gauge T-type thermocouples are attached near the heater cavity and on the Aluminum sleeve, to record the maximum hot side and cold side temperatures in the system. These readings are recorded by an NI-9213 data acquisition system, and are secondary measurements for reference purposes only. The primary temperature measurements used to characterize the thermal conductivity and thermal conductance is recorded by the infrared microscope.

RESULTS AND DISCUSSION

Data acquisition and analysis

For calibrating the emissivity, the battery is initially heated to a known uniform temperature (the reference temperature), and the radiance is measured by the infrared (IR) Microscopes sensor. Since the reference temperature is known, by comparing this radiance to that of a blackbody at the same temperature, the emissivity at each pixel is calculated for the sample, which is then used for calculating other unknown temperatures when a temperature gradient is established. Figure 4 shows a 2-dimensional temperature map, as measured by the IR microscope, with $(1024)^2$ temperature data points across a $9mm^2$ field of view. This temperature map is then imported into MATLAB, and different areas of the sample (reference region, battery region, heater region) are identified by custom image processing scripts. Since the heat transfer is radial, the temperature along any given arc inside the battery are constant, and are averaged to transform the 2-dimensional temperature map to an averaged 1-dimensional temperature map, as shown in Figure 5. For 1D radial heat transport, a logarithmic temperature decay is expected and observed.

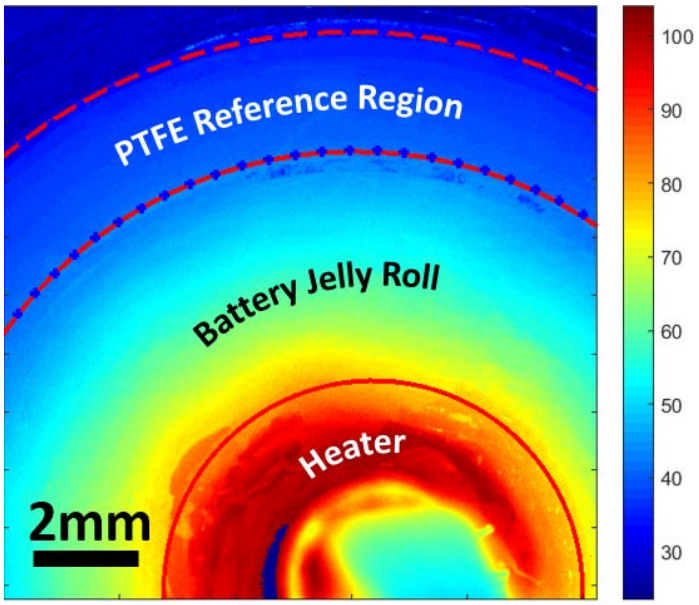

Fig. 4 A 2D temperature map of the top surface of a dry 18650 battery. Heat flows in the radial direction from the heater across the battery jellyroll and the reference layer to the heat sink. Note that the entire cross-section of the battery cannot be imaged in one experiment due to the limited field of view of the infrared microscope, and only a portion of the cell is recorded, as seen in this figure. The apparently cold area near the heater at the bottom of the image is the out of focus heater lead wires and is not included in the analysis of properties.

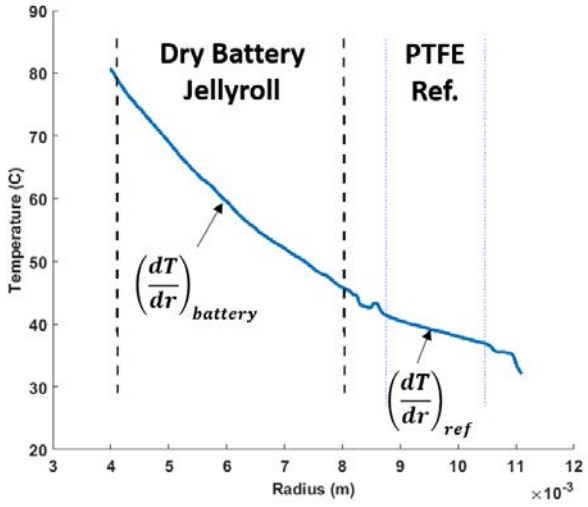

Fig. 5 The arc averaged 1D temperature profile. The temperature gradient in the reference region is used to calculate the heat rate flowing across the battery.

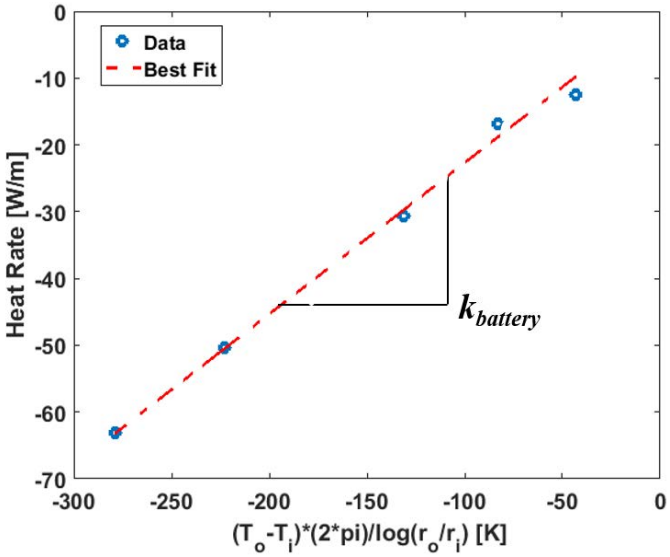

Fig. 6 Variation of the heat rate (as extracted from measurements in the reference region) with the temperature drop across the battery jellyroll scaled by a non-dimensional radius. The dotted red line is the best fit to the data points, and the slope of this best fit line gives the effective thermal conductivity of the battery. The effective thermal conductivity includes conduction through each layer and all interfacial effects within the electrode stack.

Thermal conductivity

Battery samples are prepared by assembling dry cathode and anode layers separated by the plastic separator, and then rolled together like a jelly roll cake. This jelly roll is then inserted inside the metallic case.

The temperature drop across the battery stack is recorded at various high and low side temperatures, *i.e.,* at various heat

rates. The ratio of the measured heat rate (from the reference region) with the temperature drop across the battery scaled by a non-dimensional radius yields the effective thermal conductivity of the battery, as shown in Figure 6. The effective thermal conductivity of the battery is measured to be 0.24 W/(mK) ±0.03 W/(mK). This effective thermal conductivity includes the effects of the active material, current collectors, and any interfacial effects within the stack. The effective thermal conductivity of the separator layers is calculated in a similar configuration, by making a jelly roll of just the separator material. The thermal conductivity of the separator is measured to be 0.11 W/(mK) ±0.03 W/(mK), and this value is in agreement with the values reported in literature [14].

Thermal conductance

The thermal conductance across the final layer of the jelly roll and the metallic case of the battery is not well understood, and this is the final interface across which heat needs to conduct before dissipating to the environment. To resolve this interfacial conductance, the measurements are performed with a jelly roll consisting only of the separator material, *i.e.*, the separator material is wound into a spiral roll which mimics a jelly roll, which is then inserted in the metallic case of the 18650 battery. The temperature jump at the interface of the separator and the metallic case, along with the heat rate across the system gives the thermal conductance across this interface. The results are shown in Figure 8. Experiments are repeated with 4 samples, and a large sample to sample variation is observed. With temperature, there is no statistically significant variation of thermal conductance, and hence we report a mean thermal conductance of 920 W/(m^{2}K), with a standard deviation of 470 W/(m^{2}K), which agrees well with our past work [10].

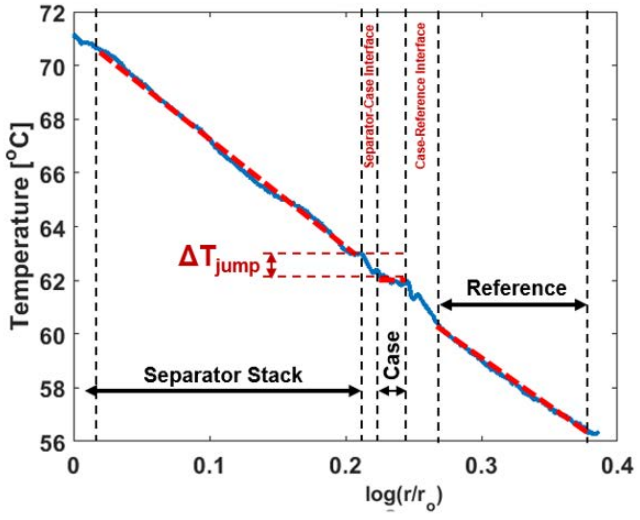

Fig. 7 The temperature profile across the separator jellyroll (stack) and the reference region, as a function of non-dimensional radius. Note the negligible temperature drop in the metallic case region, which is due to its low thermal resistance $(L/k)_{case}$, as compared to that of the separator stack.

CONCLUSIONS

To measure the thermal conductivity and thermal conductance of cylindrical 18650 cells, a cylindrical battery test rig (based on a radial version of the conventional reference bar method) has been designed, validated, and used to measure thermal properties of dry 18650 constructed in house. The effective fitted thermal conductivity of the dry 18650 battery, in a radial configuration, is measured to be 0.24 W/(mK), and that of the separator is 0.11 W/(mK). This value of thermal conductivity incorporates effects of the active electrode materials, metallic current collectors, and thermal interface resistances within the stack. Thermal conductance experiments with dry samples show large sample to sample variations, which might be due to variations in materials and contact properties (*e.g.* rough/smooth interface, pressure levels, etc.). The mean thermal conductance is measured to be 920 W/(m^{2}K), with a standard deviation of 470 W/(m^{2}K) across all samples and all case temperatures. These values are expected to be the lower bounds on the thermal conductivity and conductance, since both these properties are expected to increase in the presence of an electrolyte. This work measures the effective thermal conductivity of dry batteries in the absence of an electrolyte, whereas in an active battery, the presence of the electrolyte might provide better contact across the stack of electrodes and to the case.

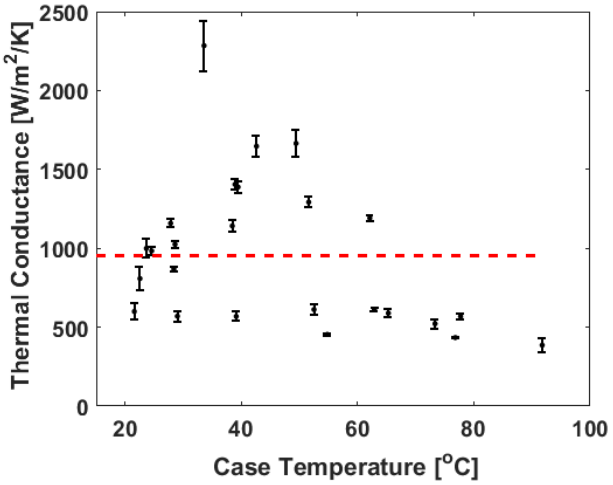

Fig. 8 Thermal conductance as a function of case temperature. The error bars represent the uncertainty in the measurement of conductance. No significant variation is seen, although some samples show a very high conductance. The dotted red line shows the mean thermal conductance across all samples and all case temperatures.

REFERENCES

[1] D. Linden, *Handbook of batteries and fuel cells*, Hamburg, Germany: McGraw-Hill Book Company GmbH, 1984.

[2] S.-I. Tobishima and J.-I. Yamaki, “A consideration of lithium cell safety,” Journal of Power Sources, vol. 81, pp. 882–886, 1999.

[3] S.-I. Tobishima, K. Takei, Y. Sakurai, and J.-i. Yamaki, “Lithium ion cell safety,” Journal of Power Sources, vol. 90, no. 2, pp. 188–195, 2000.

[4] J. Zhang, B. Wu, Z. Li, and J. Huang, “Simultaneous estimation of thermal parameters for large-format laminated lithium-ion batteries,” Journal of Power Sources, vol. 259, pp. 106–116, 2014.

[5] R. Spotnitz and J. Franklin, “Abuse behavior of high-power, lithium ion cells,” Journal of Power Sources, vol. 113, no. 1, pp. 81–100, 2003.

[6] W. Zhang, X. Zhang, C. Wang, G. Yu, and C. Yang, “Experimental and computational research on the thermal conductivities of li/socl2 batteries,” Journal of The Electrochemical Society, vol. 161, no. 5, pp. A675–A681, 2014.

[7] H. Maleki, S. A. Hallaj, J. R. Selman, R. B. Dinwiddie, and H. Wang, “Thermal Properties of Lithium Ion Battery and Components,” Journal of The Electrochemical Society, vol. 146, no. 3, pp. 947–954, 1999.

[8] J. Cho, M. D. Losego, H. G. Zhang, H. Kim, J. Zuo, I. Petrov, D. G. Cahill, and P. V. Braun, “Electrochemically tunable thermal conductivity of lithium cobalt oxide.,” Nature communications, vol. 5, no. May, p. 4035, 2014.

[9] H. Maleki, J. R. Selman, R. Dinwiddie, and H. Wang, “High thermal conductivity negative electrode material for lithium-ion batteries,” Journal of power sources, vol. 94, no. 1, pp. 26–35, 2001.

[10] A. Gaitonde, A. Nimmagadda, and A. Marconnet, “Measurement of interfacial thermal conductance in Li-ion batteries,”

[11] K. Shah, C. McKee, D. Chalise, and A. Jain, “Experimental and numerical investigation of core cooling of Li-ion cells using heat pipes,” Energy, vol. 113, pp. 852–860, 2016.

[12] Chemours.com, “Teflon chemours,” 2016. https://www.chemours.com/Teflon/en_US/.

[13] M. Pilsworth and H. Robinson, “The Thermal Conductivity of Natural Rubber,” 1971.

[14] T. E. ToolBox, “Thermal conductivity of some common materials and gases,” 2016. http://www.engineeringtoolbox.com/thermal-conductivity-d_429.html.